MRI molecular imaging monitors downstream anti-angiogenic effects of mTOR inhibition

R. Ross[1], J. L. Figueiredo[2], P. Waterman[2], R. Weissleder[3], and A. R. Guimaraes[4,5]

[1]Lank Center for Genitourinary Oncology, Dana Farber Cancer Institute, Boston, MA, United States, [2]Center for Systems Biology, Massachusetts General Hospital, Boston, mA, United States, [3]Center for Systems Biology, Massachusetts General Hospital, Boston, MA, United States, [4]Radiology, Massachusetts General Hospital/Martinos Center for Biomedical Imaging, Charlestown, MA, United States, [5]Center for Systems Biology, Massachusetts General Hospital/Martinos Center for Biomedical Imaging, Boston, mA, United States

Introduction

Renal cell carcinoma (RCC) is the third most common genitourinary tumor with an estimated number of cases numbering greater than 50,000 worldwide in 2007. The cloning of the VHL tumor suppressor gene has uncovered a role in upregulating multiple growth factors (e.g. hypoxia inducble factor-1 (HIF-1), and mammalian target of rapamycin (mTOR)), some of which may have effects on angiogenesis through upregulation of vascular endothelial growth factor (VEGF). Drugs which inhibit the vascular endothelial growth factor (VEGF) pathway, including sunitinib (Sutent®, Pfizer) and sorafenib (Nexavar®, Bayer/Onyx), as well as temsirolimus (Torisel®, Wyeth) and everolimus (Afinitor®, Novartis), inhibitors of the mammalian target of rapamycin (mTOR), have all been approved for the treatment of metastatic RCC. Recently dynamic contrast enhanced MRI (DCE-MRI) has been utilized to assess the vascular leak associated with anti-angiogenic therapies. (4; 6; 8; 9). Magnetic resonance imaging (MRI) approaches using magnetic nanoparticles (MNP) have also recently been validated for the examination of tumor vascularity *in vivo*. (2; 5) The MNP have profound T2* shortening properties with a long-lived intravascular state, which can be exploited for steady-state imaging of angiogenesis. This approach has been employed in preclinical models to monitor the anti-angiogenic effects of a vascular targeting agent in mouse models of cancer (e.g. pancreatic, fibrosarcoma). (5; 7) The aim of this study was to evaluate the in vivo effects of mTOR inhibition on the vascularity of a mouse model of RCC, comparing these effects to an established anti-angiogenic agent, sorafenib.

Methods

All studies were approved by the small animal institutional animal care and use committee at the Massachusetts General Hospital. One million CAK-1 (ATCC) cells in 100 ul Matrigel (BD Biosciences; Bedford, MA) were implanted into the right flanks of n=20 athymic nu/nu mice (MGH Cox 7). Tumors were allowed to reach the size of 500 mm^3 prior to starting any treatment protocol. All therapies (n=5/treatment arm) were given by oral gavage and included the following: a) high dose sorafenib (80 mg/kg/day); b) low dose sorafenib (30 mg/kg/day); c) rapamycin (10mg/kg/day); and d) control saline vehicle. Rapamycin was commercially available as an oral solution (1mg/ml Rapamycin) with inactive ingredients including the following: phosphatidylcholine, propylene glycol, mono- and di-glycerides, ethanol, soy fatty acids, ascorbyl palmitate and polysorbate 80. Sorafenib (200mg tablets) were crushed, weighed and then dissolved in a solution of 0.5% methylcellulose and 0.4% polysorbate-80 to produce a suspension with a final concentration of 6 mg/ml. Animals were treated daily for 28 days and then sacrificed using carbon monoxide.

Magnetic resonance imaging was performed at 4.7T on a Bruker imaging system (Pharmascan, Karlsruhe, Germany). Animals were imaged at baseline and weekly until the termination of therapy. Animals were anesthetized during imaging with 1-1.5 inhaled Isofluorane, and monitored during imaging with respiratory monitoring. Multi-slice multiecho (MSME) T2-weighted imaging was performed prior to and following intravenous injection of magnetic nanoparticle (MNP)(10mg/kg Fe). The following parameters were utilized: Flip angle = 90^0; Matrix size (128 x 64); TR = 2500msec.; TE = 16 equally spaced echoes at 8.6msec. intervals ranging from 8.6msec. to 137msec; field of view (FOV) = 4.24 x 2.12 cm, slice thickness = 1mm. Vascular volume fractions (VVF) measures were calculated from the pre- and post-contrast MNP enhanced images as described in detail elsewhere (1-3). A fundamental assumption is that the change in the transverse relaxation rate ($\Delta R2=1/\Delta T2$)) relative to the pre-injection baseline is proportional to the perfused local blood volume per unit tumor volume (V) multiplied by a function (*f*) of the plasma concentration of the agent (P). $\Delta R2 = k \cdot f(P) \cdot V$. R2 was fit by using a mono-exponential fitting algorithm for the multi-TE data (Osirix and converted to absolute tumoral VVF by scaling measurements to muscle with a known VVF of 3%. Data are reported as VVF +/- standard error of the mean. Statistical analysis using a two-tailed paired t-test, compared different time points for each treatment paradigm (GraphPad Prism 4.0, La Jolla, CA).

After 28 days of therapy, animals were sacrificed and tumors assessed for histologic, quantitative analysis including CD31 staining (microvessel density)MVD), VEGF, and polyclonal phospho-p70 S6 kinase (mTOR). To determine microvessel density (MVD) three representative sections per tumor were analyzed. Results are reported as mean vessel number ± SD per 20x high power field. Linear regression analysis compared MRI VVF measurements to MVD. Statistical analysis using a two-tailed unpaired t-test, compared each treatment paradigm (GraphPad Prism 4.0, La Jolla, CA).

Results:

Figure 1 demonstrates T1-weighted MRI of mice with pseudocolorized VVF maps superimposed over the center of the tumor within the right flank for each treatment arm (rapamycin (top row), sorafenib (middle row), and control (bottom row)) of the trial at baseline, and at the end of therapy. Note the heterogeneity of signal intensity and color spread throughout all cohorts at baseline, with marked decrease in vascularity in the rapamycin (top row) and sorafenib (high dose – middle row) treated animals as compared to control (bottom row). Of note, only 3 mice survived all 3 weeks of therapy within the rapamycin treated arm. VVF was quantified and graphed each week in each cohort and graphed (mean +/- SEM) (Figure 1d). Note the parallel, rapid decrease in VVF in both the sorafenib and rapamycin treated cohorts as compared to control with a statistically significant decrease in VVF ($p<0.05$) at week 3 relative in both cohorts relative to differences noted in the control cohort. Although there was a decrease in mean VVF in control mice, there was no statistically significant difference in VVF comparing week 3 to baseline measurements in control mice. MRI VVF measurements also demonstrated dose response differences between low and high dose sorafenib most notable and exceptional at week 2, but these differences did not demonstrate statistical significance (Fig. 1e). Histologic analysis (Fig 14f,g,h) demonstrates statistically significant differences in p70 staining and VEGF staining comparing rapamycin treated to control mice values ($p<0.0001$) . As well, there were statistically significant differences in p70 and VEGF staining comparing sorafenib treated mice to rapamycin treated mice ($p<0.0001$, labeled +). Interestingly, however, there was a statistically significant difference in p70 staining comparing sorafenib treated mice to control mice ($p<0.001$, labeled *).

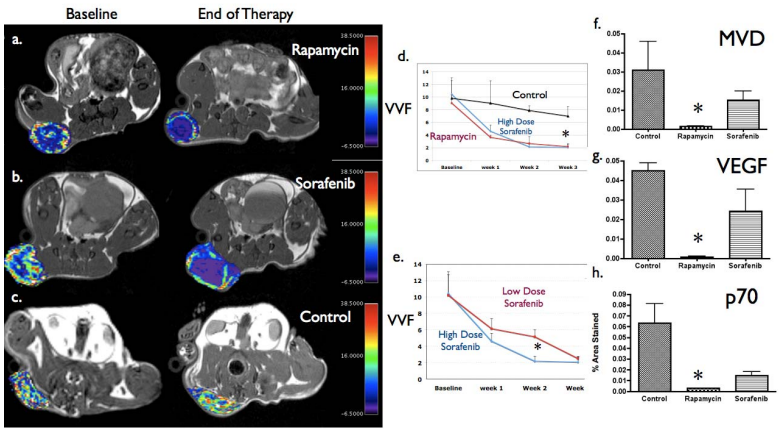

Discussion:

In summary, our results demonstrate that MRI measures of VVF quantify microvascular changes following targeted therapies. MRI VVF correlates highly to histopathologic indices of microvessel density (MVD) and may serve as a surrogate marker of angiogenesis confirming previous results. Furthermore, the sensitivity of this technique may provide physiological insight into potential downstream anti-angiogenic effects associated with other chemotherapeutic strategies, as well as may serve as an preclinical outcome measure of dose scheduling given the accuracy in discriminating between low and high dose dosing schedules (2; 5; 10).

References:

1. Boxerman, J. et al. (1995). Magnetic Resonance in Medicine **34**:555-566
2. Bremer, C. et al. (2003). Radiology **226**:214-220
3. Dennie, J. et al. (1998). Magnetic Resonance in Medicine **40**:793-799
4. Flaherty, K. T. et al. (2008). Cancer Biol Ther **7**:496-501
5. Guimaraes, A. R. et al. (2008). Pancreas **37**:440-444
6. Lane, H. A. et al. (2009). Clin Cancer Res **15**:1612-1622
7. Persigehl, T. et al. (2007). Radiology **244**:449-456
8. Rosen, M. A.; Schnall, M. D. (2007). Clin Cancer Res **13**:770s-776s
9. Schnell, C. R. et al. (2008). Cancer Res **68**:6598-6607
10. Tang, Y. et al. (2005). Cancer Res **65**:8324-8330